

Tuning Crystalline Structure of Zeolitic Metal–Organic Frameworks by Supersonic Spraying of Nanoparticle Suspension Precursors

Bhavana N. Joshi,^{1,†} Jong-Gun Lee,^{1,†} Do-Yeon Kim,¹ Jong-Hyuk Lee¹, Ji Sun Lee,² Young Kyu Hwang,² Jong-San Chang,^{2,3} Salem Al-Deyab,⁴ Jin-Chong Tan,^{5,*} Sam S. Yoon^{1,*}

¹School of Mechanical Engineering, Korea University, Seoul 136-713, Republic of Korea

²Res. Group for Nanocatalysts, Korea Res. Inst. of Chem. Tech., Daejeon 305-600, Republic of Korea

³Dept. of Chem., Sungkyunkwan University, Suwon 440-476, Republic of Korea

⁴Petrochem. Research Chair, Dept. of Chem., King Saud Univ., Riyadh 11451, Saudi Arabia

⁵Dept. of Engineering Science, University of Oxford, Parks Road, Oxford OX1 3PJ, United Kingdom

Abstract

The deposition of a sodalite Zeolitic Imidazolate Framework-7 (ZIF7) films by a supersonic cold-spraying technique has been successfully accomplished for the first time. The high-speed impact of supersonic cold spraying increased the monodispersed peak in the ZIF7 crystalline structure. However, the intensity of the structural change decreased with increasing amounts of nylon in the ZIF7 suspension. Nylon was originally intended to improve the adhesion of the ZIF7 particles onto the substrate. Mitigation of phase-change in ZIF7 can be attributed to impact dampening conferred by the polymeric nature of nylon, which preserved the original three-dimensional crystalline structure of ZIF7. The inclusion of *N,N*-dimethylformamide (DMF) in a nylon–ZIF7 suspension improved the dispersion of ZIF7 nanoparticles, which in turn eliminated the dampening effect from the nylon and recovered the distinctive monodispersity peak arising from the high-speed impact. This distinctive peak was observed at all impact speeds when the ZIF7 suspension contained DMF. At the highest impact speed, amorphization of the film was observed, resulting from the severe pulverization of nanoparticles upon impacting the substrate. We show that high-rate cold spraying of ZIF7 particles can be combined with nylon and other pressure-transmitting media to control the formation of three distinctive phases (I, II and III). The unique capability to tune the crystalline structure of ZIF7 is important to customize the film functionality needed for specific applications.

Keywords: Supersonic spraying, Metal organic framework, Phase transformation, Zeolitic imidazolate framework, Mechanical properties

[†]These authors have contributed equally.*

Corresponding authors: skyoon@korea.ac.kr, jin-chong.tan@eng.ox.ac.uk

1. Introduction

Zeolitic imidazolate frameworks (ZIFs) are 3-D assemblies of metal ions and imidazole-based organic ligands, whose porous open frameworks are mimicking those of (inorganic) aluminosilicate zeolites. The crystal structure of ZIFs is analogous to that of zeolites due to the bond-angle resemblance between metal–linker–metal bonds and the Si–O–Si linkages, both of which subtending a bond angle of 145° [1]. The combination of metal and organic linkers in ZIFs yields porous materials with high surface areas and tunable functionalities, along with a good combination of thermal and chemical stability. Thus, they can potentially be used in different practical applications such as sensors, catalysts, adsorbents, matrix fillers, membranes, and drug delivery. [2-4].

ZIF7 is formed by linking benzimidazolate (bIm) anions to divalent Zn^{2+} cations. First discovered by Huang et al. [5], it has a sodalite topology with hexagonal symmetry [6]. ZIF7 is distinct from ZIF8 which also adopts a sodalite topology, due to the presence of a phenyl group in the bIm ligand of the former structure [7]. The pore window of ZIF7 is 0.30 – 0.35 nm, and thus it allows access to CO_2 molecules over N_2 , showing high selectivity for CO_2 [8]. ZIF7 is capable of CO_2 separation from NO_2 [8] at relatively low pressures and temperatures and alkanes/alkenes through a gate-opening process [9]. ZIFs display structural flexibility because of their weaker

coordination bonds, in fact the mechanical properties of ZIFs (Young's modulus, hardness and bulk modulus) [10] are approximately a factor of ten times lower than those of inorganic zeolites [11]. Because of the flexibility of the framework, ZIFs can undergo structural transformation or phase changes under high pressures or temperatures, as well as after adsorption of gas molecules. Aguaoda et al. [12] and Zhao et al. [13] described the transformation of large-pore ZIF7 to narrow-pore ZIF7 due to gas adsorption induced by temperature and pressure, respectively. Wharmby et al. [14] recently reported the porous to dense phase transition of desolvated ZIF4. The phase transition in ZIF4 is due to the rotation of imidazolate linkers, resulting in pore volumetric contraction. Collective lattice dynamics (THz vibrations) and soft modes present in ZIF7 can also give rise to gate-opening phenomenon, and trigger mechanical instability causing shear induced structural collapse and framework amorphization [15].

The crystal morphology of metal–organic frameworks (MOFs) can be controlled by selecting particular synthesis conditions or processing routes. For example in a paper by Low et al. [16], it was demonstrated that the crystal–to–crystal phase transformation occurs when ZIF-L crystals are transformed to ZIF-8 crystals under different solvents and heating processes. This transformation is called a topotactic phase transition, in which a crystalline material undergoes structural changes but the final phase is related to the initial crystal structure by its similar crystallography or orientation.

Synthesizing ZIF7 as films or membranes on porous alumina or polymer-based membranes [17] makes such films attractive for sensors, adsorption and gas separation applications [2] [18] [19]. For the fabrication of ZIF membranes and films, the main approaches used are direct synthesis and secondary growth methods. However, very few methods are reported for the deposition of ZIF7 films [20]. Melgar et al. [1] deposited ZIF7 films by an electrospray technique

on an alumina substrate and observed the formation of ZnO when the substrate temperature was maintained at 160°C. Peng et al. [21] reported the fabrication of ZIF7 molecular sieve nanosheets that were exfoliated by using wet ball milling; the membranes were then deposited on porous α -Al₂O₃ substrates. The prepared membranes were subsequently used for hydrogen gas permeance and selectivity. However, these methods are not easily scalable for use in commercial production and industry.

Herein, we report for the first time the use of cold spraying for the deposition of ZIF7 films, a method which is fast and highly scalable [22, 23]. In the cold-spraying technique, particles are injected into a supersonic gas stream and accelerated to supersonic velocities. These high-velocity particles collide with the substrate with substantial kinetic impact energy, resulting in strong adhesion of the particles to substrate. Thus, this is a high-rate coating method, the apparatus details of which were discussed in an earlier report [24]. The goal of this investigation was to study the influence of cold-spray impact pressure and effects of different solvents on the structural properties of ZIF7. We have discovered distinctive changes to the crystalline structure upon supersonic impact of ZIF7 particles, with and without application of nylon and *N,N*-dimethylformamide (DMF) in the suspension precursors.

2. Experimental Methodology

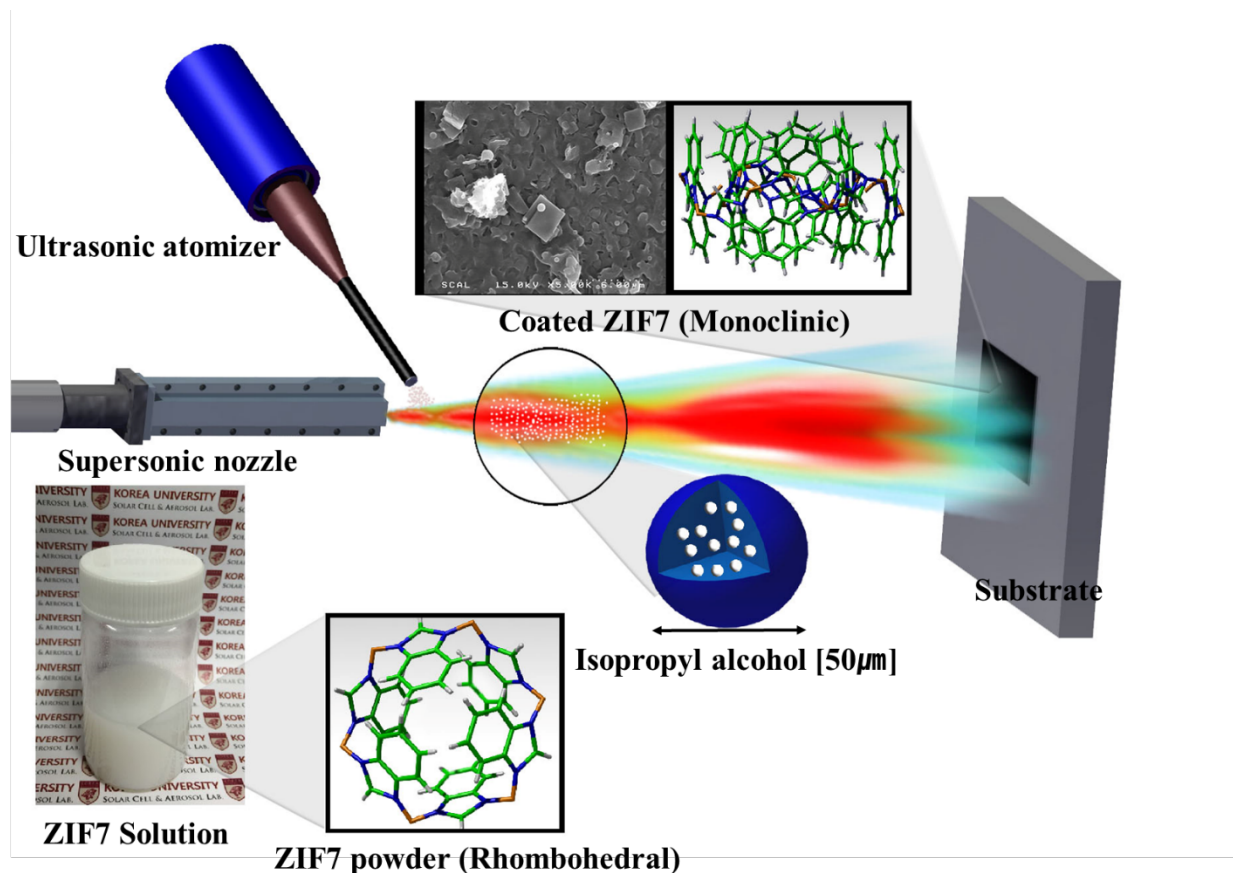


Figure 1. Graphical illustration of the supersonic cold-spraying ZIF7 process.

2.1 Suspension precursors

ZIF7 nanoparticles were suspended in various types of solvents and sprayed onto a copper substrate via supersonic cold spraying. Three different sets of colloidal solutions were prepared each using 1 g of ZIF7 powder. The first suspension was ZIF7 in 50 mL of isopropyl alcohol (IPA), denoted as I-ZIF7. In the second suspension, various concentration (1 and 6 wt%) of nylon-6 was added to the I-ZIF7 solution, denoted as N-ZIF7. To improve dispersion of the ZIF7 nanoparticles,

we added 10 mL of DMF to the N-ZIF7 solution, denoted as D-ZIF7. These three types of suspensions were sonicated (Pronextech, South Korea) for 2 min to achieve a homogenous dispersion of ZIF7 nanoparticles in the solution prior to cold spraying.

2.2 Supersonic cold spraying

The ZIF7 films were deposited by means of a supersonic spray-coating system (also known as the cold-spray method), as shown in the schematic in **Figure 1**, by using ZIF7 powder (powder particle size 100–150 nm). A typical cold-spray system consists of a gas tank, gas heater, supersonic nozzle, ultrasonic atomizer, syringe pump, and an X–Y translation stage [25].

The prepared precursor was pumped by a syringe pump (KDS LEGATO 210, Sercrim Lab. Tech. South Korea) toward the nozzle via an ultrasonic liquid processor (VCS134ATFT, Sonic & Materials, Inc., USA). The feed solution was discharged in an undifferentiated, supersonic air stream through the nozzle, which accelerated the sol toward the substrate; a uniform coating was generated by means of four cycles of deposition. The operating air pressure (P_0) was varied from 2–7 bar and the heater temperature (T_0) for the air was varied from 150–450°C. The ZIF7 nanoparticles gained high kinetic energy by the hot compressed air blown through the supersonic nozzle, which yielded well-adhered, compact ZIF7 films on the substrates. The ZIF7 films were coated onto copper substrates with an average thickness of *ca.* 20 μm .

2.3 Materials characterization

The structural phase transformations of ZIF7 were studied using an X-ray diffractometer (Rigaku, SmartLab). The surface morphology and surface roughness of the deposited films were determined using a high-resolution scanning electron microscope (HR-SEM, S-5100, Hitachi Co., Japan) and an atomic force microscope (AFM, XE-100, Park Systems, Korea), respectively. The thermal stability of the films was measured using a thermogravimetric analyzer (TGA, Q-500, TA Instruments, USA).

3. Results and Discussion

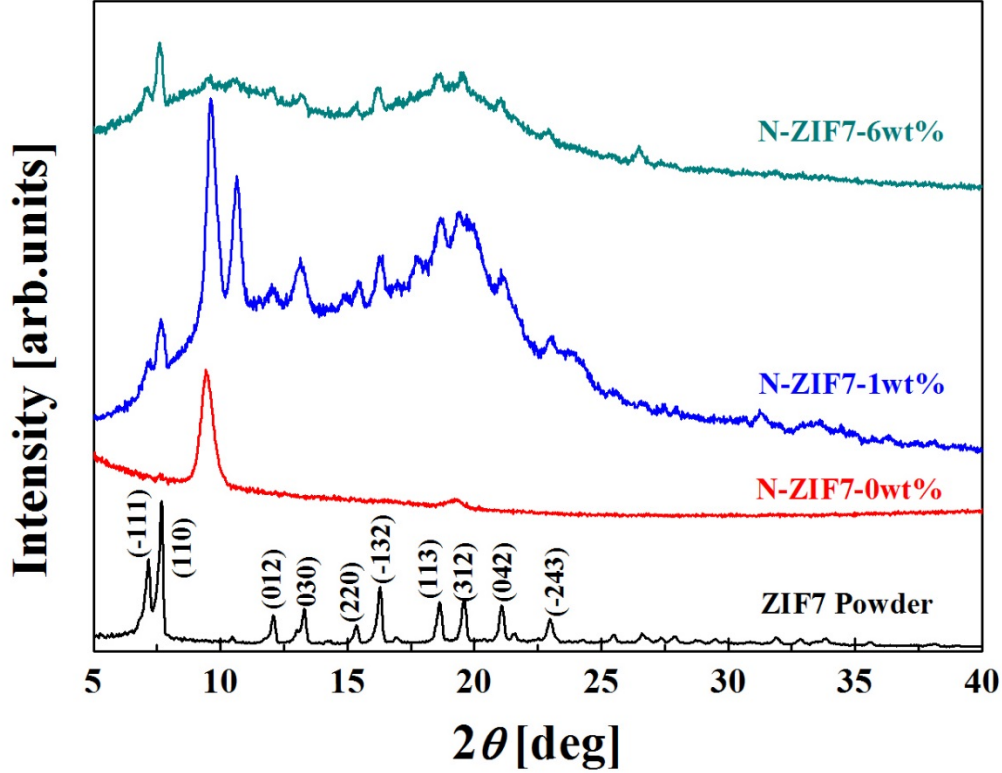


Figure 2. XRD patterns showing the effect of nylon concentration from 0 to 6 wt% on film crystal structures.

The crystal structures of the cold-sprayed ZIF7 powder and ZIF7 films with varying concentrations of nylon (0, 1, and 6 wt%) were identified by X-ray diffraction (XRD), and the results are shown in **Figure 2**. The XRD pattern of the pristine ZIF7 powder (as synthesized) exhibits characteristic peaks at $2\theta = 7.15, 7.65, 12.09, 13.03, 15.37, 18.64, 19.60, 21.10$, and 23° , corresponding to the specific Miller indices in **Figure 2**, confirming that it is ZIF7 Phase I. The nylon used in the solvent and films was deposited at $P_0 = 2$ bar and $T_0 = 250^\circ\text{C}$. Without the nylon

content, the IPA solvent is expected to have evaporated because of the high temperature and pressure and ZIF7 impacting on substrate with high speed and thus transforming to a completely different phase. This phase shows an intense peak at $2\theta = 9.6^\circ$, which matches well with the ZIF7 Phase III reported by Zhao et al. [13]. ZIF7 Phase III features a two-dimensional (2D) layered architecture which is significantly denser and more stable [26] compared with porous structure of phase I. Peng et al. [21] applied ball milling to ZIF7 nanoparticles and suggested that the 3D phase III transformed to a 2D structure due to the breaking of coordination bonds in the six-membered rings of ZIF7, thereby leaving behind a framework containing only four-membered rings. They described this resultant phase as the 2D stacking of ZIF7 layers along the (002)-oriented *c*-axis. Indeed, this delamination process occurred because of (lower energy) impact deformation using wet ball milling of ZIF7 carried out for the purpose of nanosheet exfoliation. In the current study, it is proposed that high velocity mechanical impact will facilitate the aforementioned 3D to 2D framework conversion step. We reasoned that a combination of shear and compressive stresses coming from high velocity impact has resulted in formation of ZIF7 Phase III, as evidenced from the strongly textured film with (002) facets corresponding to the very distinct 2θ peak at 9.6° (**Figure 2**).

When the nylon concentration in the suspension precursor was 1 wt%, the phase changed from polycrystalline ZIF7 (Phase I) to mixed-phase ZIF7 (Phase II), which showed peaks at $2\theta = 9.6$ and 10.51° , along with the other peaks matching those of the phase I in ZIF7, which resemble those of the pure powder. This mixed-phase peaks of ZIF7 are consistent with the peaks of ZIF7 Phase II reported by Zhao et al. [13], who applied thermal heating at 427°C to yield the phase change. When the concentration of nylon is increased to 6 wt%, phase I is preserved as confirmed by the Bragg peak at 7.5° . These results may be due to the nylon acting as an intermolecular binder

that lowers the impact pressure on ZIF7 by forming a protective sac, thereby improving the overall mechanical stability of nanoparticles as explained in the next section. When the nylon concentration is low, the ZIF7 particles will be impacting the substrate with partial pressure; however, nylon still plays some role in lowering the effect of impact during particle-to-substrate collision, and thus the phase transformation obtained appears to be of mixed-phase ZIF7.

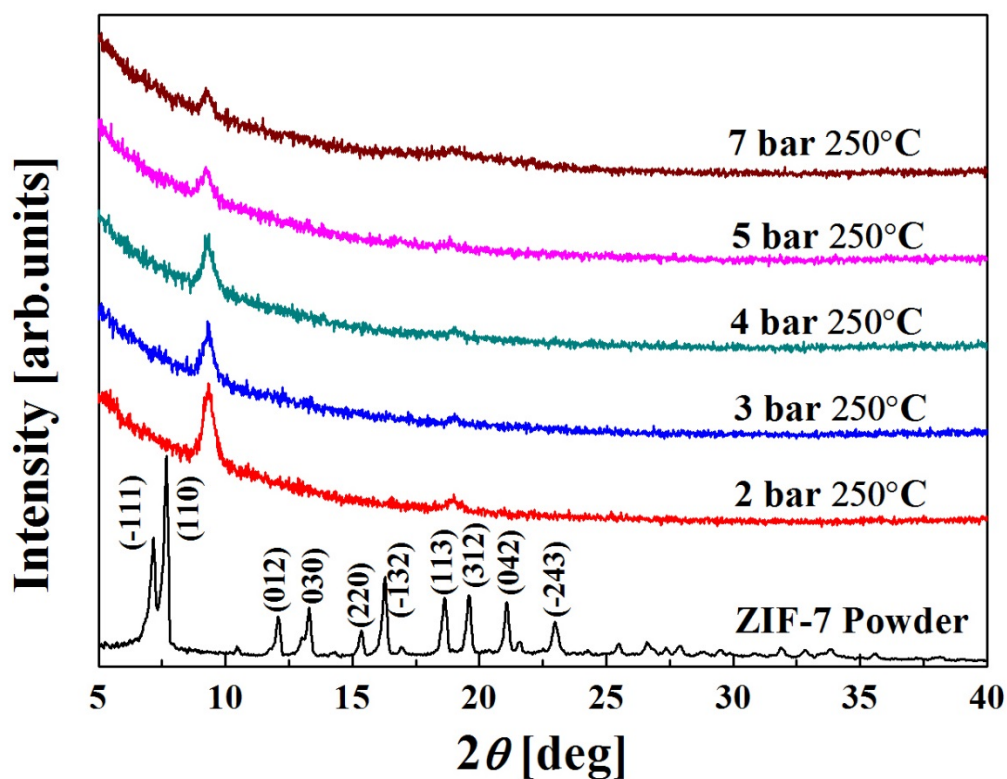


Figure 3. XRD patterns of the film crystal structures of the I-ZIF7 precursor (without nylon) at supersonic cold-spray pressures of 2–7 bar.

When dispersed in IPA in the absence of nylon, the ZIF7 particles underwent a structural transformation directly to Phase III, as shown in **Figure 3**, showing the important effect of the impact pressure generated by supersonic cold spraying. The intense peak appearing at 9.6° at $P_0 = 2$ bar systematically weakens at an increasingly higher pressures due to the gradual loss in long-

range ordering (crystallinity) of the ZIF7 structure. The poor crystalline structure of ZIF7 is because of the collapse of the framework due to collisions of ZIF7 particles with the substrate at very high impact velocities and elevated strain rates, for which we suggest is the result of thermo-mechanical deformation causing structural collapse responsible for the amorphisation process [27] [28]. The particles injected into the supersonic air stream coming through the de Laval nozzle attain velocities ranging from 300 to 500 m/s depending on the pressure and temperature. Such high impact pressures facilitate the adhesion of particles on the substrate, but they also induce fractures in the particles, as mentioned in our previous study [22].

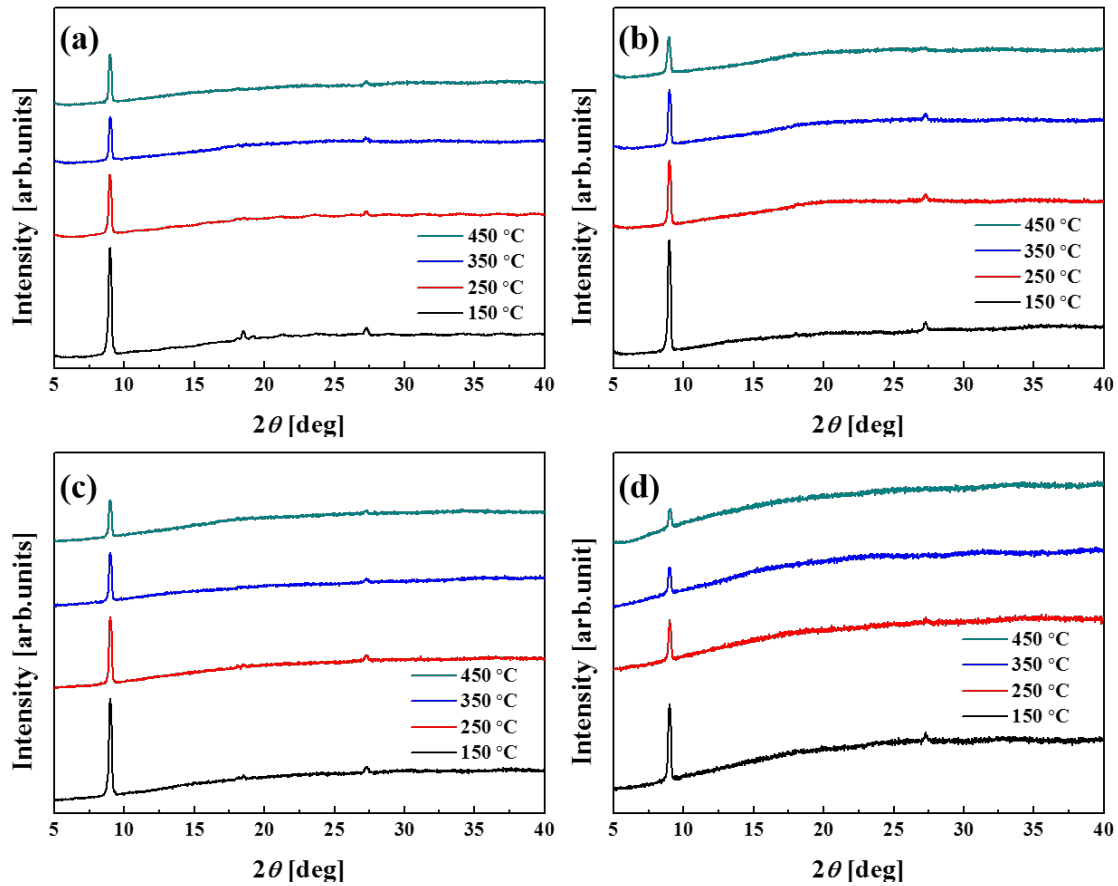


Figure 4. XRD patterns of film crystal structures of D-ZIF7 with 6 wt% nylon at varying operating temperatures and pressures of (a) 2, (b) 3, (c) 4, and (d) 5 bar.

We established that the use of DMF in the colloidal solution improved the dispersion of ZIF7 nanoparticles. The XRD pattern presented in **Figure 4** clearly reveals that the inclusion of DMF in the N-ZIF7 suspension minimized the effect of nylon, thus recovering the original XRD peaks of the pure ZIF7 powder. Phase III [13, 21] is confirmed by the dominant peak appearing at $2\theta = 9.6^\circ$. Thus, it is clear that DMF directly acts as a pressure-transmitting fluid. There was no significant effect of IPA, nylon, or both on the phase transformation, and thus the effect of high-speed pulverization of the supersonic spray is the dominant mechanism that causes the phase transformation. As compared to I-ZIF7 in **Figure 3**, importantly the inclusion of nylon and DMF in the suspension precursor also reduced the amorphization rate of ZIF7, both of which thus improve the mechanical stability of ZIF7 nanoparticle by enhancing its structural resistance against pore collapse under impact stress. It is noteworthy that the formation of ZnO is indicative of an increase in density. This ZnO formation is often induced when carbon degrades at high processing temperatures, in which case the porous MOF structure begins to collapse, forming the dense structure. Although supersonic cold spraying is carried out at high gas temperatures, all of this thermal energy is converted into kinetic energy, and thus the static temperature near the substrate location is slightly higher than room temperature. This low processing temperature (namely, supersonic “cold” spraying) prevents the formation of ZnO.

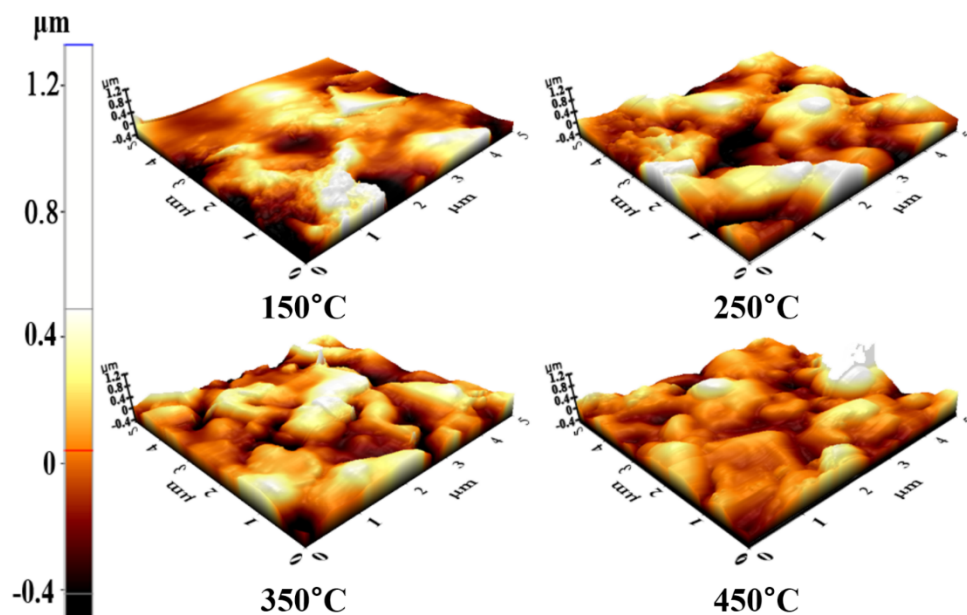


Figure 5. Surface roughness from AFM images of the cold-sprayed films at various impact speeds controlled by the operating gas temperature ($150^{\circ}\text{C} \leq T_0 \leq 450^{\circ}\text{C}$). The gas pressure was fixed at $P_0 = 2$ bar.

The 3D AFM morphologies of D-ZIF7 films deposited at $P_0 = 2$ bar at different temperatures are presented in **Figure 5**. The peaks and valleys in the AFM image are ascribed to random lateral ZIF7 stacking. The films clearly show increasing surface roughness with decreasing particle size, which varied with varying high impact energy of the supersonic cold spraying. The arithmetical mean roughness values (R_a) determined from the AFM images are shown in **Figure 6(a)**. The roughness increased with increasing air temperature, whereas the ten-point median roughness (R_z) values are observed to vary significantly. **Figure 6(b)** shows the surface areas of the uncoated copper substrate and the films deposited at increasing temperatures and a constant pressure of $P_0 = 2$ bar as measured using AFM [28]. The surface area increases with increasing T_0 ,

which also increases the impact velocity and pressure by converting the greater thermal energy into kinetic energy. As a result, particle pulverization increases with increasing T_0 .

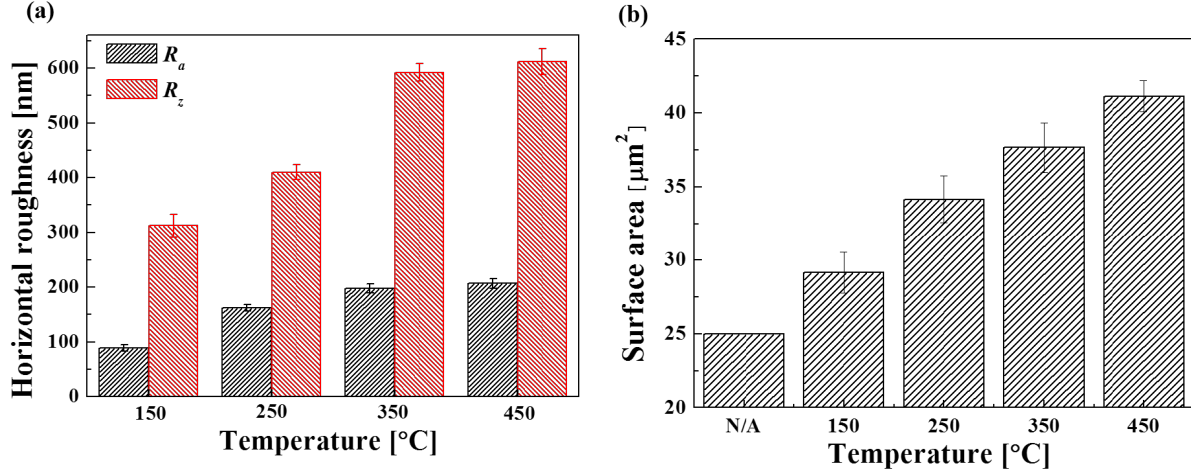


Figure 6. (a) Surface roughness and (b) area of ZIF7 films for $150^\circ\text{C} \leq T_0 \leq 450^\circ\text{C}$. The gas pressure was fixed at $P_0 = 2$ bar.

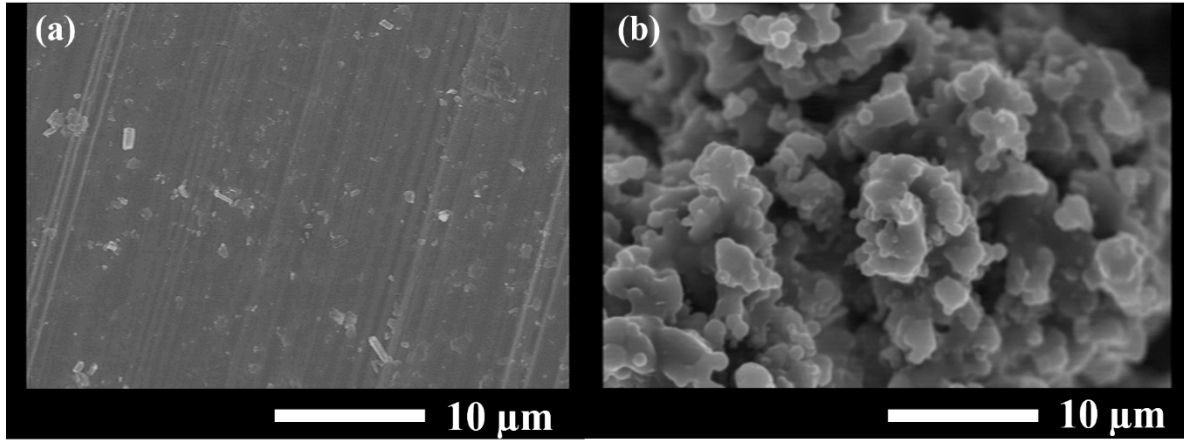


Figure 7. SEM images of (a) I-ZIF7 and (b) N-ZIF7 films at a nylon concentration of 6 wt%. The operating temperature and pressure were $T_0 = 250^\circ\text{C}$ and $P_0 = 2$ bar, respectively. DMF was not included in the suspension precursors.

Figure 7 shows the SEM images of I-ZIF7 and N-ZIF7. For the I-ZIF7 film, the surface morphology shows small ZIF7 particles, with some flat surfaces due to the high impact pressure of the cold spraying. On the other hand, for the N-ZIF7 film, the surface morphology shows agglomerates comprising polycrystalline ZIF7 particles, as evidently shown in **Figure 2**. This is because nylon acts as an intermolecular binder that mechanically stabilizes the 3D structural of ZIF7 (phase I). The polymeric nylon provides a “cushioning” effect that reduces the intensity of the pulverization process, as evident in **Figure 7(b)**.

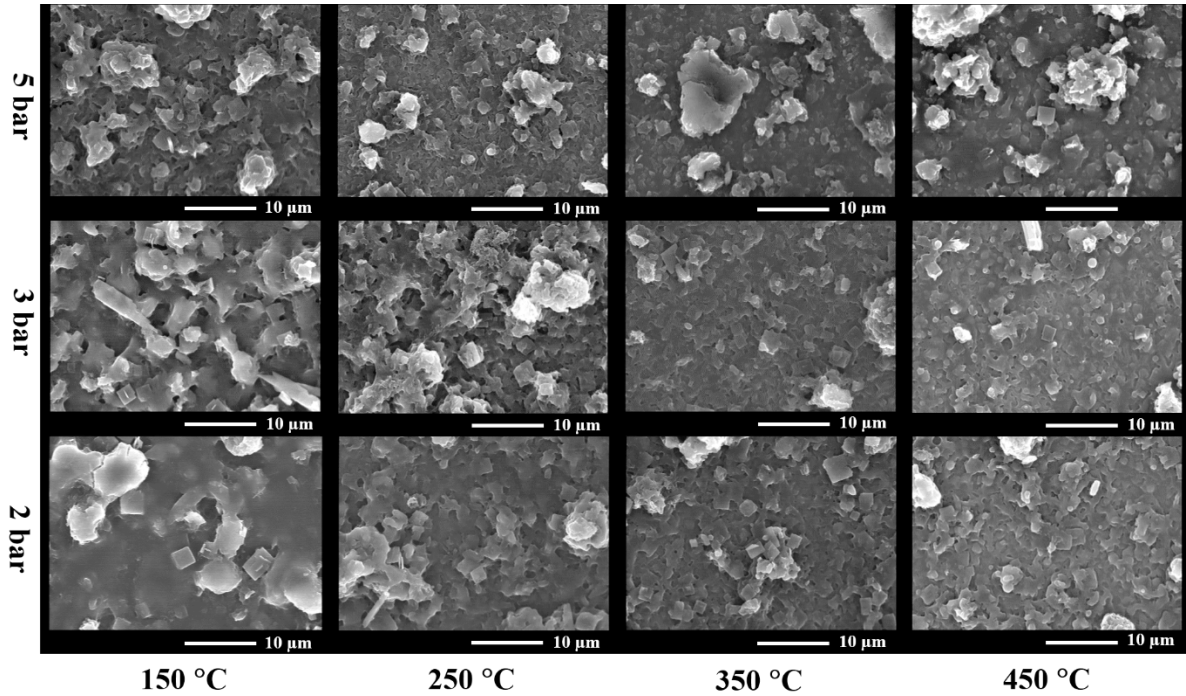


Figure 8. SEM images showing the effect of impact speed on the surface morphology of D-ZIF7 films. The gas temperature and pressure varied in the range of $150^{\circ}\text{C} \leq T_0 \leq 450^{\circ}\text{C}$ and $2 \text{ bar} \leq P_0 \leq 5 \text{ bar}$, respectively.

Figure 8 shows SEM images of cold-sprayed D-ZIF7 films on a copper substrate at $P_0 = 2 \text{ bar}$ and different temperatures. Cubic-shaped ZIF7 particles are clearly observed up to $P_0 = 2\text{--}3$

bar. A thin layer of nylon and DMF covering the ZIF7 grains, resulting in a stiff material, is observed in all SEM images. This stiff material is melted, fractured, or both by the high impact energy of the particles. However, the grains of ZIF7 observed in the SEM images of films deposited at high air pressures and temperatures are fractured and flattened as a result of impact pressure. The images clearly show the change in surface microstructure with increasing gas pressure. Less porous and more agglomerated surface microstructures are observed at an air pressure of 5 bar. Comparing the SEM image of D-ZIF7 at $T_0 = 250^\circ\text{C}$ and $P_0 = 2$ bar in **Figure 8** with **Figure 7(b)** (N-ZIF7), the effect of DMF inclusion is clear. The particle impact speed in the two cases was the same because both sets of data were acquired at the same operating temperature and pressure. As mentioned earlier, the surface morphology was much rougher when using N-ZIF7 because of the “cushioning” effect of nylon. When DMF was used, because of the improved dispersion of the particles in the suspension precursor, the pulverization process upon particle impact was much more efficient, resulting in a relatively uniform surface morphology.

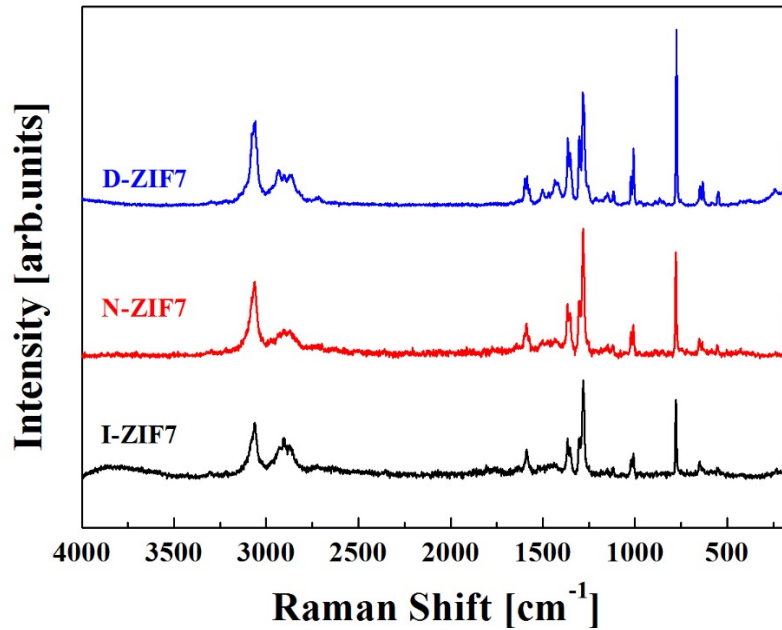


Figure 9. Raman spectra of ZIF7 films with nylon and DMF. The pressure and temperature were fixed at $P_0 = 2$ bar and $T_0 = 250^\circ\text{C}$, respectively.

The Raman spectra of ZIF7 films deposited with different solution configurations are presented in **Figure 9**. The peaks correspond to the different vibrations of the Zn–N lattice, benzene, and the imidazole ring. A comparison of the ZIF7 Raman data with the results reported by Zhao et al. [13] shows that the peaks are in good agreement. **Table 1** presents the Raman frequencies and their respective band assignments. However, after spray deposition, the intensity of the Zn–N bond peak weakens, which may be result of mechanical straining of the compliant ZnN_4 tetrahedral coordination environment prevalent in ZIF structures [29] [30]. **Figure 9** shows that all Raman bands remain similar and at constant frequencies, indicating that the chemical structure of ZIF7 remains unperturbed.

Table 1. Raman frequency and band assignment.

Frequency [cm^{-1}]	Band Assignment
140	Zn-N
551	Stretching of benzene & imidazole ring
554	Stretching of benzene & imidazole ring
650	Torsion of imidazole ring
773	Bending of benzene & imidazole ring
1007	Bending of benzene ring
1268	Bending of benzene & imidazole C-H
1351	Stretching of C-N
1573	Bending of N-H
2900-3050	Stretching of C-H in benzene
3050-3150	Stretching of C-H in imidazole

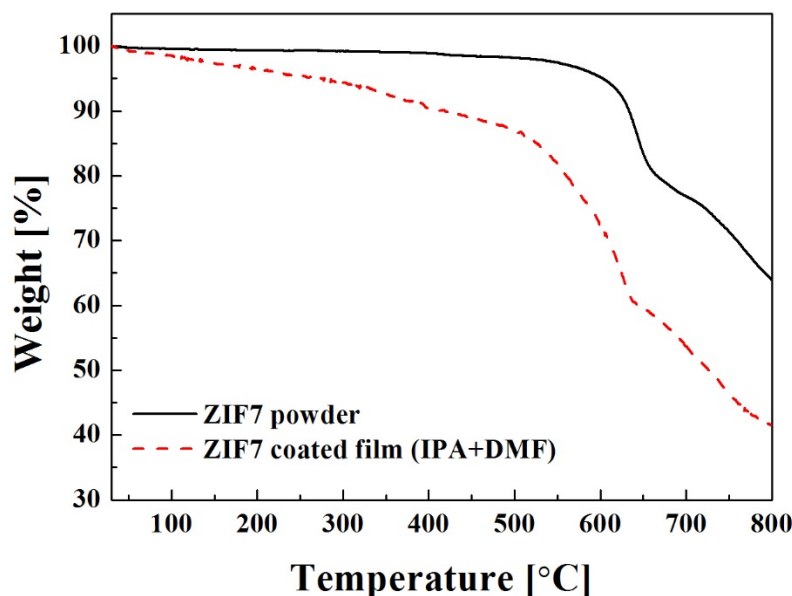
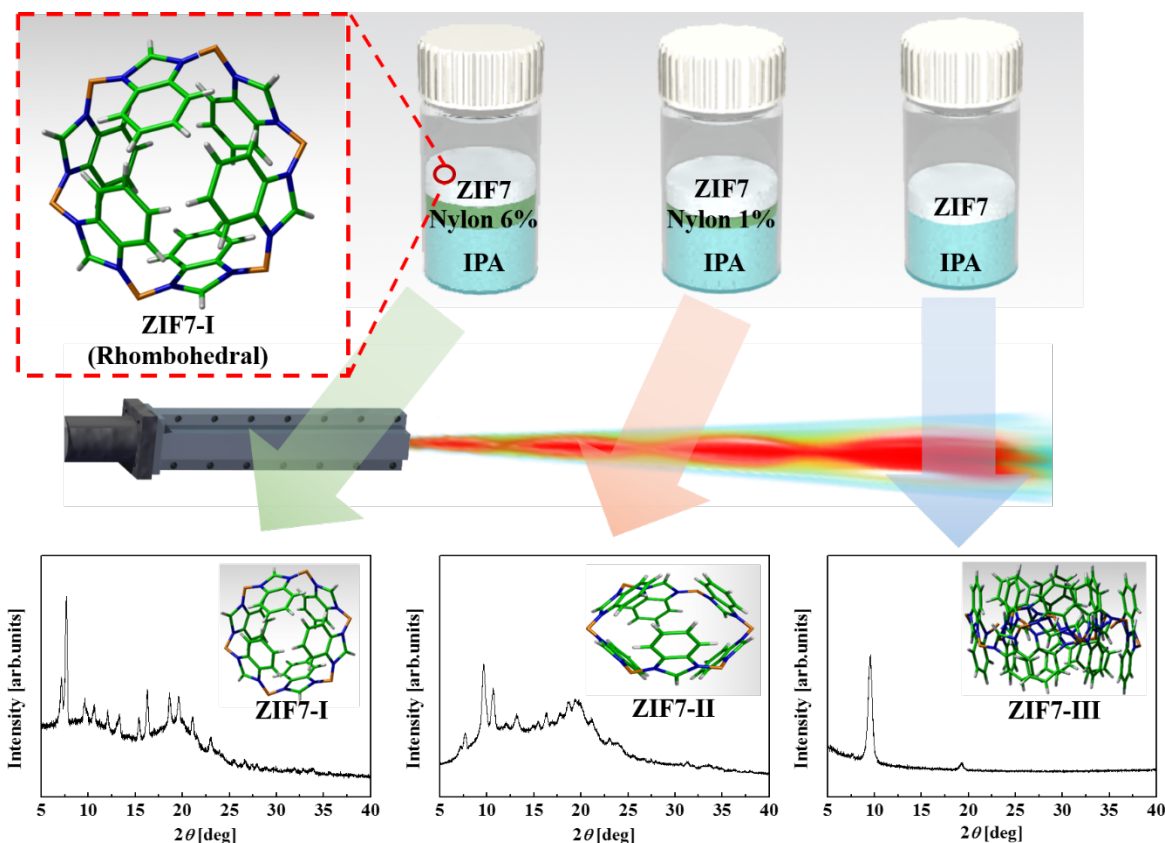


Figure 10. Thermogravimetric analysis of pure ZIF7 powder and D-ZIF film without nylon.

The TGA data shown in **Figure 10** indirectly indicates the role of DMF regarding the collapse and retention of the crystal structure. Note that the D-ZIF7 film did not include nylon, in order to elucidate the effect of DMF alone. The thermal stability test of the pure ZIF7 powder and the D-ZIF7 film by TGA was carried out under nitrogen gas at a heating rate of 10°C/min. **Figure 10** shows three gradual steps in the weight loss for the D-ZIF7 film at 25°C and 800°C. Approximately 5% weight loss is observed between 25°C and 300°C because of the removal of moisture and trapped alcohol. A weight loss of 35% is observed between 300°C and 630°C due to the removal of DMF. The weight loss observed between 630°C and 800°C indicates the thermal decomposition of the structural framework of ZIF7 associated with the decomposition of the organic linkers. For the pure ZIF7 powder, 70% residue remained. However, for the D-ZIF7 film,

the remaining residue was 42%. This difference between 70% and 42% is because of the structural change of the film due to the high-speed impact.



Scheme 1. The change in the crystalline structure of the supersonically sprayed ZIF7 films with varying nylon concentration.

The mechanism of phase transition due to cold spraying is summarized in **Scheme 1**. The ZIF7 structure (Phase I) shows negligible no phase change at a nylon concentration of 6 wt%, as confirmed by XRD. If the nylon concentration is lowered, i.e., 1 wt%, the ZIF7 particles hit the substrate with partial pressure because a small amount of nylon in solution reduces the collision impact of the particles on the substrate, giving rise to ZIF7 Phase II, where PXRD data indicate

that the majority of the six- and four-membered rings of ZIF7 are mechanically strained or stretched but likely only a few of the framework bonds break. When only IPA solvent is used, the solvent evaporates under the high temperature and pressure of the supersonic air flow, and ZIF7 particles will impact on the substrate at very high speed and energy, giving rise to Phase III due to delamination of the 3D structure to the 2D ZIF7 structure. The transformation from 3D to 2D frameworks occurs due to the breaking of coordination bonds in the six-membered ZIF7 ring and the formation of four-membered rings, as explained by Peng et al. [21]. Our results demonstrate that nylon could act as an efficient intermolecular binder that lowers the impact pressure on ZIF7, thereby improving porous framework mechanical stability for avoiding any unwanted phase changes.

4. Conclusion

The 3D crystal structure of ZIF7 powder underwent a phase transformation from polycrystalline porous to crystalline dense due to particle pulverization into a 2D phase because of the high-speed impact of the powder by supersonic cold spraying. By tuning the crystal structures of ZIF7 via the supersonic spraying, customized films can be fabricated to meet the needs of various applications in permeance and gas separation. This is the first attempt to deposit ZIF7 films by supersonic spraying, and the structural response of ZIF7 to the high-pressure impact is evident. Inclusion of 6 wt% of nylon in the precursor solvent resulted in the deposition of ZIF7 films with the original polycrystalline structure, i.e., one that was similar to that of the pure powder. The absence of nylon gave rise to the phase transformation. This study provides a better understanding of the cold-spray deposition of ZIF7 films and provides a scalable deposition method for fabricating porous and dense MOF films depending on the requirements of the application. This method also makes it possible to manufacture amorphous ZIF films with significant applications in chemically functionalized hybrid glass materials.

References

- [1] V.M. Aceituno Melgar, H.T. Kwon, J. Kim. Direct spraying approach for synthesis of ZIF-7 membranes by electrospray deposition, *Journal of Membrane Science* 459 (2014) 190-196.
- [2] T. Li, Y. Pan, K.-V. Peinemann, Z. Lai. Carbon dioxide selective mixed matrix composite membrane containing ZIF-7 nano-fillers, *Journal of Membrane Science* 425–426 (2013) 235-242.
- [3] X. Wu, M. Niknam Shahrak, B. Yuan, S. Deng. Synthesis and characterization of zeolitic imidazolate framework ZIF-7 for CO₂ and CH₄ separation, *Microporous and Mesoporous Materials* 190 (2014) 189-196.
- [4] W. Cai, T. Lee, M. Lee, W. Cho, D.-Y. Han, N. Choi, A.C.K. Yip, J. Choi. Thermal Structural Transitions and Carbon Dioxide Adsorption Properties of Zeolitic Imidazolate Framework-7 (ZIF-7), *Journal of the American Chemical Society* 136 (2014) 7961-7971.
- [5] X. Huang, J. Zhang, X. Chen. [Zn(bim)₂] · (H₂O)_{1.67}: A metal-organic open-framework with sodalite topology, *Chinese Science Bulletin* 48 (2003) 1531-1534.
- [6] Y. Li, F. Liang, H. Bux, W. Yang, J. Caro. Zeolitic imidazolate framework ZIF-7 based molecular sieve membrane for hydrogen separation, *Journal of Membrane Science* 354 (2010) 48-54.
- [7] P. Zhao, G.I. Lampronti, G.O. Lloyd, E. Suard, S.A. Redfern. Direct visualisation of carbon dioxide adsorption in gate-opening zeolitic imidazolate framework ZIF-7, *Journal of Materials Chemistry A* 2 (2014) 620-623.
- [8] J. Xie, N. Yan, F. Liu, Z. Qu, S. Yang, P. Liu. CO₂ adsorption performance of ZIF-7 and its endurance in flue gas components, *Frontiers of Environmental Science & Engineering* 8 (2014) 162-168.
- [9] C. Gücüyener, J. van den Bergh, J. Gascon, F. Kapteijn. Ethane/Ethene Separation Turned on Its Head: Selective Ethane Adsorption on the Metal–Organic Framework ZIF-7 through a Gate-Opening Mechanism, *Journal of the American Chemical Society* 132 (2010) 17704-17706.
- [10] J.C. Tan, T.D. Bennett, A.K. Cheetham. Chemical structure, network topology, and porosity effects on the mechanical properties of Zeolitic Imidazolate Frameworks, *Proceedings of the National Academy of Sciences* 107 (2010) 9938-9943.
- [11] J.C. Tan, A.K. Cheetham. Mechanical properties of hybrid inorganic–organic framework materials: establishing fundamental structure–property relationships, *Chemical Society Reviews* 40 (2011) 1059-1080.
- [12] S. Aguado, G. Bergeret, M.P. Titus, V. Moizan, C. Nieto-Draghi, N. Bats, D. Farrusseng. Guest-induced gate-opening of a zeolite imidazolate framework, *New Journal of Chemistry* 35 (2011) 546-550.
- [13] P. Zhao, G.I. Lampronti, G.O. Lloyd, M.T. Wharmby, S. Facq, A.K. Cheetham, S.A. Redfern. Phase Transitions in Zeolitic Imidazolate Framework 7: The Importance of Framework Flexibility and Guest-Induced Instability, *Chemistry of Materials* 26 (2014) 1767-1769.
- [14] M.T. Wharmby, S. Henke, T.D. Bennett, S.R. Bajpe, I. Schwedler, S.P. Thompson, F. Gozzo, P. Simoncic, C. Mellot-Draznieks, H. Tao. Extreme Flexibility in a Zeolitic Imidazolate Framework: Porous to Dense Phase Transition in Desolvated ZIF-4, *Angewandte Chemie* 127 (2015) 6547-6551.
- [15] M.R. Ryder, B. Civalleri, T.D. Bennett, S. Henke, S. Rudić, G. Cinque, F. Fernandez-Alonso, J.-C. Tan. Identifying the Role of Terahertz Vibrations in Metal-Organic Frameworks: From Gate-Opening Phenomenon to Shear-Driven Structural Destabilization, *Physical review letters* 113 (2014) 215502.
- [16] Z.-X. Low, J. Yao, Q. Liu, M. He, Z. Wang, A.K. Suresh, J. Bellare, H. Wang. Crystal transformation in zeolitic-imidazolate framework, *Crystal Growth & Design* 14 (2014) 6589-6598.
- [17] B. Zornoza, C. Tellez, J. Coronas, J. Gascon, F. Kapteijn. Metal organic framework based mixed matrix membranes: An increasingly important field of research with a large application potential, *Microporous and Mesoporous Materials* 166 (2013) 67-78.
- [18] A. Bétard, R.A. Fischer. Metal–Organic Framework Thin Films: From Fundamentals to Applications, *Chemical Reviews* 112 (2012) 1055-1083.

- [19] M.D. Allendorf, V. Stavila. Crystal engineering, structure–function relationships, and the future of metal–organic frameworks, *CrystEngComm* 17 (2015) 229-246.
- [20] J. Yao, H. Wang. Zeolitic imidazolate framework composite membranes and thin films: synthesis and applications, *Chem Soc Rev* 43 (2014) 4470-4493.
- [21] Y. Peng, Y. Li, Y. Ban, H. Jin, W. Jiao, X. Liu, W. Yang. Metal-organic framework nanosheets as building blocks for molecular sieving membranes, *Science* 346 (2014) 1356-1359.
- [22] J.-G. Lee, D.-Y. Kim, B. Kang, D. Kim, S.S. Al-Deyab, S.C. James, S.S. Yoon. Thin film metallization by supersonic spraying of copper and nickel nanoparticles on a silicon substrate, *Computational Materials Science* 108 (2015) 114-120.
- [23] D.Y. Kim, J.G. Lee, B.N. Joshi, S.S. Latthe, S.S. Al-Deyab, S.S. Yoon. Self-cleaning superhydrophobic films by supersonic-spraying polytetrafluoroethylene–titania nanoparticles, *Journal of Materials Chemistry A* (2015).
- [24] D.-Y. Kim, J.-J. Park, J.-G. Lee, D. Kim, S.J. Tark, S. Ahn, J.H. Yun, J. Gwak, K.H. Yoon, S. Chandra, S.S. Yoon. Cold Spray Deposition of Copper Electrodes on Silicon and Glass Substrates, *Journal of thermal spray technology* 22 (2013) 1092-1102.
- [25] D.Y. Kim, S. Sinha-Ray, J.J. Park, J.G. Lee, Y.H. Cha, S.H. Bae, J.H. Ahn, Y.C. Jung, S.M. Kim, A.L. Yarin. Self-Healing Reduced Graphene Oxide Films by Supersonic Kinetic Spraying, *Advanced Functional Materials* 24 (2014) 4986-4995.
- [26] Q.-F. Yang, X.-B. Cui, J.-H. Yu, J. Lu, X.-Y. Yu, X. Zhang, J.-Q. Xu, Q. Hou, T.-G. Wang. A series of metal–organic complexes constructed from in situ generated organic amines, *CrystEngComm* 10 (2008) 1534-1541.
- [27] T.D. Bennett, D.A. Keen, J.-C. Tan, E.R. Barney, A.L. Goodwin, A.K. Cheetham. Thermal Amorphization of Zeolitic Imidazolate Frameworks, *Angewandte Chemie International Edition* 50 (2011) 3067-3071.
- [28] T.D. Bennett, S. Cao, J.C. Tan, D.A. Keen, E.G. Bithell, P.J. Beldon, T. Friscic, A.K. Cheetham. Facile Mechanochemical Synthesis of Amorphous Zeolitic Imidazolate Frameworks, *Journal of the American Chemical Society* 133 (2011) 14546-14549.
- [29] J.-C. Tan, B. Civalleri, C.-C. Lin, L. Valenzano, R. Galvelis, P.-F. Chen, T.D. Bennett, C. Mellot-Draznieks, C.M. Zicovich-Wilson, A.K. Cheetham. Exceptionally Low Shear Modulus in a Prototypical Imidazole-Based Metal-Organic Framework, *Physical review letters* 108 (2012) 095502.
- [30] J.-C. Tan, B. Civalleri, A. Erba, E. Albanese. Quantum mechanical predictions to elucidate the anisotropic elastic properties of zeolitic imidazolate frameworks: ZIF-4 vs. ZIF-zni, *CrystEngComm* 17 (2015) 375-382.